ADVANCED MATERIALS

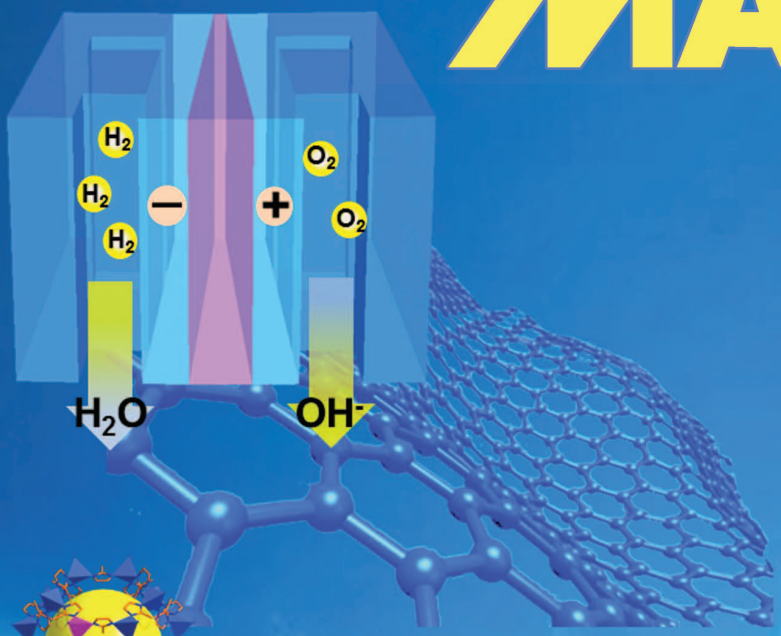

METAL–ORGANIC FRAMEWORKS

Bimetallic metal–organic frameworks are rationally synthesized by Y. Xiong, H.-L. Jiang, and co-workers on page 5010 as templates for porous carbons via facile pyrolysis. The optimized porous carbon with high surface area and multicomponent active dopants exhibits excellent electrocatalytic performance for the oxygen reduction reaction, which is even better than that of the Pt/C catalyst in alkaline media.

WILEY-VCH

ADVANCED MATERIALS
www.advmat.de

Materials Views
www.MaterialsViews.com

From Bimetallic Metal-Organic Framework to Porous Carbon: High Surface Area and Multicomponent Active Dopants for Excellent Electrocatalysis

Yu-Zhen Chen, Chengming Wang, Zhen-Yu Wu, Yujie Xiong, Qiang Xu, Shu-Hong Yu, and Hai-Long Jiang**

Porous carbons have stimulated a great deal of interest due to their low-cost, chemical stability, good electrical conductivity, and potential applications in diverse fields, such as gas adsorption/storage, electrode materials, and catalyst supports.[1] It has been demonstrated that heteroatom doping (e.g., N, B, P, Co, Fe, etc.) within the skeleton of porous carbons is a powerful approach to tuning electronic properties or/and conductivity, which thus facilitate their applications, particularly in electrode materials.[2,3] High surface area and uniform doping are considered to be crucial to the performance of carbon materials.[2e,3a] To this end, metal-organic frameworks (MOFs),[4] constructed by metal (clusters) and carboxylate or/and N-involved ligand with huge diversity, intuitively should be a class of ideal precursors. The well-organized framework can be converted to carbon with uniform heteroatom decoration, and the long-range ordering and high porosity of MOFs can be partially preserved to afford high surface area of resultant porous carbons via facile pyrolysis.[5,6] Since our early work on this subject,[5a,b] a number of MOF-derived porous carbon materials have been developed for various applications, especially for oxygen reduction reaction (ORR),[6] an important reaction for fuel cells that expects to avoid or minimize the use of precious metals such as Pt.[1g,7,8]

With great progress achieved, the following concerns are recognized to be critical to ORR, while not simultaneously realized yet in any MOF-derived carbon: (1) high surface area and hierarchical pores guarantee the free diffusion of O_2 and electrolyte to the catalytic active sites and their short diffusion path lengths; (2) homogeneous distribution of heteroatoms, especially N, is pivotal to electrocatalysis;[8a] (3) involvement of Co(Fe)–N_x moiety would provide valid active sites;[8a,g] (4) graphitized carbon, which is usually formed via catalysis over Fe, Co, etc., would enhance electrical conductivity. To meet the above challenges, zeolitic imidazolate frameworks (ZIFs),[9,10] a subclass of MOFs, have been identified as precursors as they are rich in carbon, nitrogen, and transition metals, and can be readily prepared at low cost. The ZIF-8[9] has been well demonstrated to afford high-surface-area carbons with high N content by us and others,[5b,c,6d,e] whereas it cannot provide critical Co(Fe)–N_x sites and good graphitized carbon. To address these issues, Co-based ZIF-67,[10] isostructural to ZIF-8, should be a suitable candidate but can only offer carbon with low surface area and porosity.

Bearing these in mind, a series of bimetallic ZIFs (BMZIFs) based on ZIF-8 and ZIF-67 with varied ratios of Zn/Co, have been successfully prepared in this work as they are lattice-matched. The unprecedented BMZIF-templated porous carbons, inheriting both merits of carbons independently from ZIF-8 and ZIF-67, possess large surface area, high graphitization degree, and highly dispersed N and CoN_x active species, which have not been simultaneously achieved in any previous MOF-derived porous carbon.[5,6] Remarkably, the optimized BMZIF-derived carbon exhibits excellent ORR activity approaching the level of commercial Pt/C in alkaline media. Strikingly, upon further doping with additional phosphorus, it possesses not only better ORR catalytic activity, but also superior stability and tolerance to methanol compared to Pt/C catalyst (**Scheme 1**). To the best of our knowledge, the obtained impressive performance in terms of half-wave potential has not been achieved in all previous MOF-derived porous carbons and most noble-metal free materials.[2c–f,6,8] Meanwhile, our study suggests that the CoN_x, high surface area and hierarchical pores, high graphitization as well as N, P dopants are all beneficial to the superb ORR activity.

The BMZIFs (designated as BMZIF-*n*, *n* indicates the molar ratio of Zn/Co) were synthesized via the room-temperature reaction of a $Zn(NO_3)_2$ and $Co(NO_3)_2$ mixture solution and 2-methylimidazole in methanol (Scheme S1, Supporting Information). As the molar ratio of Zn/Co decreases, the color of the obtained BMZIFs gradually changed from white to purple while the color of all particles from one batch kept consistent, reflecting the uniform distribution of Co^{2+} and Zn^{2+} ions in BMZIFs (Figure S1, Supporting Information). The inductively coupled plasma atomic emission spectrometry (ICP-AES) analysis for BMZIF-20 as a representative indicates the actual value of Zn/Co molar ratio is 17.8, which is close to the

Y.-Z. Chen, Dr. C. Wang, Z.-Y. Wu, Prof. Y. Xiong, Prof. S.-H. Yu, Prof. H.-L. Jiang
Hefei National Laboratory for Physical Sciences at the Microscale
Key Laboratory of Soft Matter Chemistry
Chinese Academy of Sciences
Collaborative Innovation Center of Suzhou Nano Science and Technology
Department of Chemistry
University of Science and Technology of China
Hefei, Anhui 230026, P. R. China
E-mail: yjxiong@ustc.edu.cn; jianglab@ustc.edu.cn
Prof. Q. Xu
National Institute of Advanced Industrial Science and Technology (AIST)
Ikeda, Osaka 563-8577, Japan

DOI: 10.1002/adma.201502315

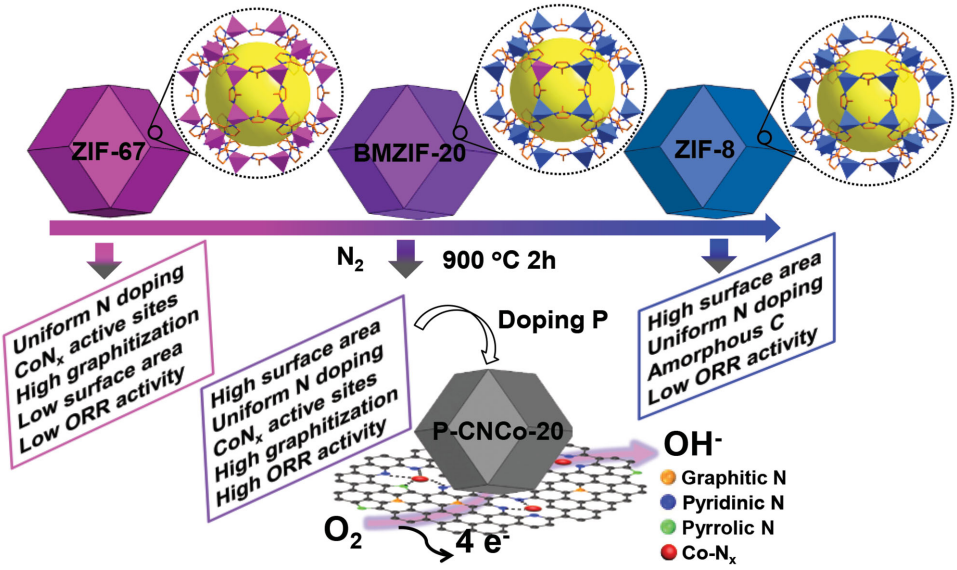

Scheme 1. Schematic illustration for the preparation of porous carbons from BMZIFs for highly efficient oxygen reduction reaction.

theoretical value (20). The SEM images show that the well-dispersed BMZIF nanocrystals in polyhedral shape with sizes basically increase from ≈50 to ≈400 nm as the Zn/Co molar ratios decrease (Figure S2, Supporting Information). However, it is interesting to find that the sizes of BMZIF-20 and -40 are ≈30 nm (**Figure 1**a, Figure S2b, Supporting Information), even smaller than that of ZIF-8. The uniform distribution of Co^{2+} and Zn^{2+} ions in BMZIFs has been further proven by elemental mapping for one representative BMZIF-20 crystal, in which Zn and Co species are coexisted and highly dispersed (Figure S3, Supporting Information). Powder XRD patterns of all BMZIFs match well with simulated ZIF-8 and ZIF-67 owing to their similar unit cells and crystal lattices (Figure S4, Supporting Information). The N_2 sorption curves suggest that BMZIF-20 has similar microporous features to those in ZIF-8 and ZIF-67 (Figure S5, Supporting Information). Unexpectedly, taking BMZIF-20 as a representative, BMZIFs exhibit markedly better water stability than ZIF-67 (Figure S6, Supporting Information), which would be greatly beneficial to its practical applications.

The BMZIFs as templates/precursors underwent pyrolysis at 900 °C under N_2 to afford Co, N-doped porous carbons. In this process, the generated ZnO was reduced by carbon to give evaporative Zn at such high temperature.[5a,b] The products were stirred with 0.5 M H_2SO_4 at 80 °C to remove the inactive and unstable Co species as far as possible to afford CNCo-*n* (*n* means the same to that in BMZIF-*n*; *n* = 100 and 0 relate to carbon derived from ZIF-8 and ZIF-67, respectively). The SEM images (Figure 1b, Figure S7, Supporting Information) show that the CNCo-*n* particles are well dispersed and have retained sizes and morphology from their precursors, BMZIFs.

Elemental mapping indicates that CNCo-20 is mainly composed of C, N, and Co, among which N and Co are dispersed uniformly throughout the carbon matrix (Figure 1c), demonstrating the niche of MOF precursors. The presence of a few Co in CNCo-*n* has been also demonstrated by the ICP-AES (Table S1, Supporting Information). The residual Co species should originate from two components: (1) a small amount of Co nanoparticles (NPs) tightly wrapped by graphitic carbon; (2) stable CoN_x moieties inherited from the CoN_4 units in BMZIF precursors. The overlapped Co/N signals and well dispersed Co species in the carbon matrix suggest Co might be stabilized by N coordination to Co–N_x moiety (Figure 1c).[8d–f] Both types of Co species have been previously proved to merit the ORR.[11]

The TEM images for CNCo-20 suggest the absence of aggregated large Co NPs in the porous carbon (Figure 1d, Figure S8a, Supporting Information). TEM and HRTEM images of CNCo-20 show the abundant graphitic carbon structures with interplane spacing of (002) crystal lattice (3.4 Å) that should be ascribed to the catalytic graphitization behavior of Co NPs (Figure 1e, Figure S8, Supporting Information).[5h] Powder XRD patterns for all carbon materials exhibit two peaks at ≈25° and 44° indexed to (002) and (101) diffractions of carbon (Figure 1f). The strong (002) peak in CNCo-20 shifts toward a comparatively sharp peak at 26°, in stark contrast to the broad peak at ≈23° of CNCo-100. This result suggests the improved graphitization degree in CNCo-20.[5h,6b] The result is further supported by the lower I_D/I_G value of CNCo-20 than that of CNCo-100 in Raman spectra (Figure S9, Supporting Information). The XRD peaks located at around 44° and 51° are assignable to the (111) and (200) diffractions of *fcc* Co originated from the Co NPs embedded in carbon shell (Figure 1e inset), as indicated above.

The porous texture of CNCo-*n* has been characterized by N_2 sorption at 77 K (Figure 1g), which reveals their large pore volumes and the coexistence of micropore and mesopore, as indicated by pore size distributions (Figure S10, Supporting Information). The BET surface areas are 270, 362, 550, 1090, 1225, 1480, and 2184 $m^2\ g^{-1}$ for CNCo-*n* with n equal to 0, 0.2, 5, 10, 20, 40, and 100, respectively, exceeding most of the metal doped-carbon materials derived from MOFs.[6a–c,f–l] The large surface area and pore volume would be beneficial to the exposure of active sites and rapid transportation of ORR-relevant species. The high-resolution X-ray photoelectron spectroscopy

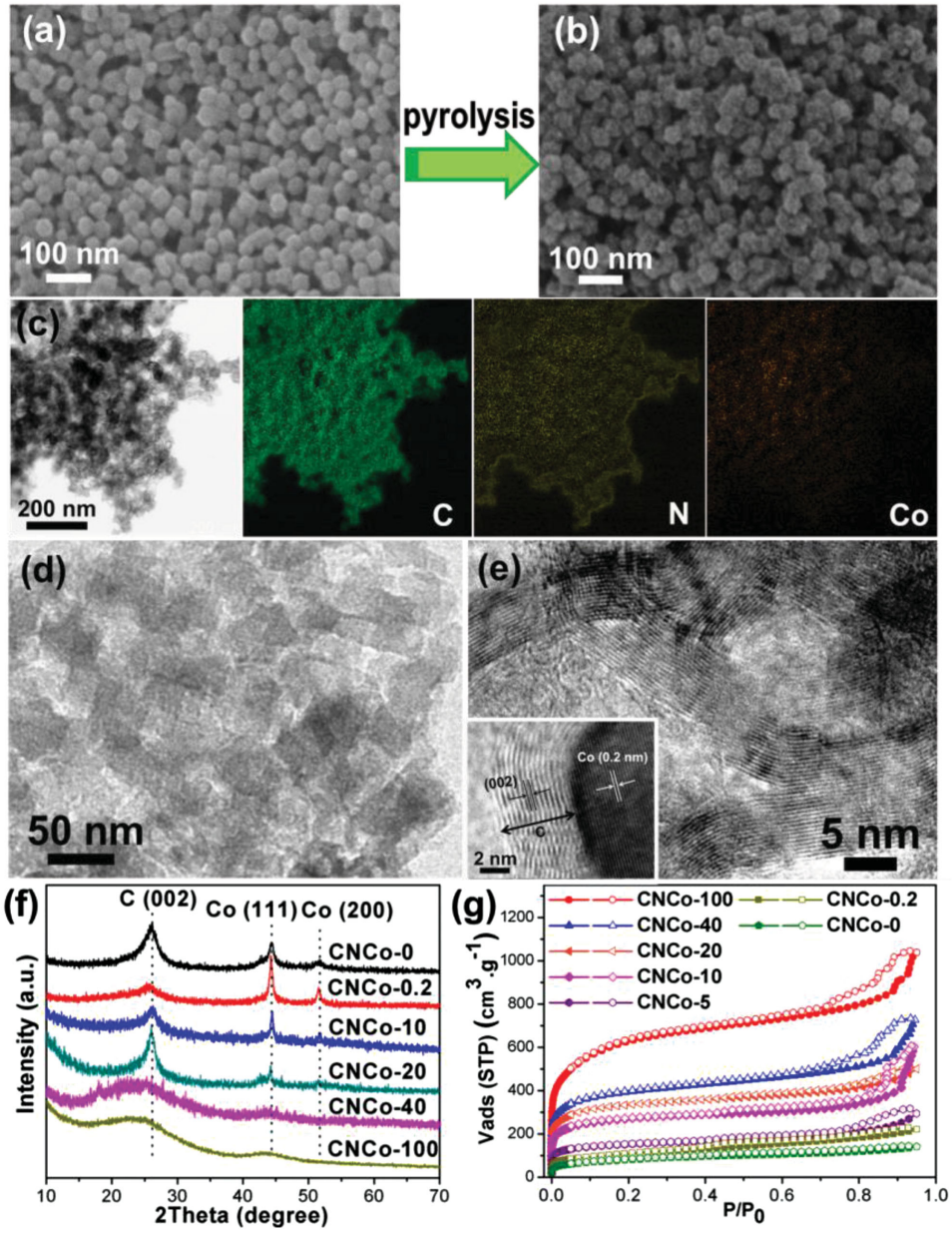

Figure 1. Scanning electron microscopy (SEM) images of a) BMZIF-20 and b) CNCo-20. c) Transmission electron microscopy (TEM) image of CNCo-20 and the corresponding elemental mapping of C, N, and Co. d,e) Enlarged TEM images of CNCo-20 (inset in (e): HRTEM image showing Co NP tightly wrapped by the well-developed graphitization layers). f) Powder XRD patterns and g) N_2 sorption isotherms for CNCo-*n* samples.

(XPS) spectra for N 1s in CNCo-20 exhibit five types of nitrogen species: dominant graphitic-N and also Co-N_x, pyridinic-N, pyrrolic-N as well as oxidized-N (Figure S11a, Supporting Information). It has been reported that all these N atoms play crucial roles in the ORR process except for the oxidized N. The high-resolution Co 2p spectrum presents three important forms of Co species, namely, metallic Co, CoO_x or CoC_xN_y, and Co–N_x (Figure S11b, Supporting Information).[12] This finding demonstrates the presence of Co–N_x, which has been identified as one of the best active sites for ORR.

Given that phosphorus (P) doping in carbon is one of the most effective solutions to create competent ORR active sites,[2e] the P element was introduced into CNCo-20 by annealing with triphenylphosphine in N_2 atmosphere to give P-CNCo-20. The XPS spectra of P 2p for P-CNCo-20 indicate that P atoms have been successfully incorporated (Figure S12, Supporting Information). The two types of P at 132.7 and 133.8 eV are assignable to P–C and P–O bonding, respectively. The peaks for N 1s and Co 2p in P-CNCo-20 are nearly the same to those in CNCo-20, revealing the retained structure upon P doping.

With desirable structural information indicated above, we investigate the ORR activity of CNCo-*n* catalysts in alkali media, as fuel cells are usually operated under basic conditions for practical application and industrial production,[7a,f] The cyclic

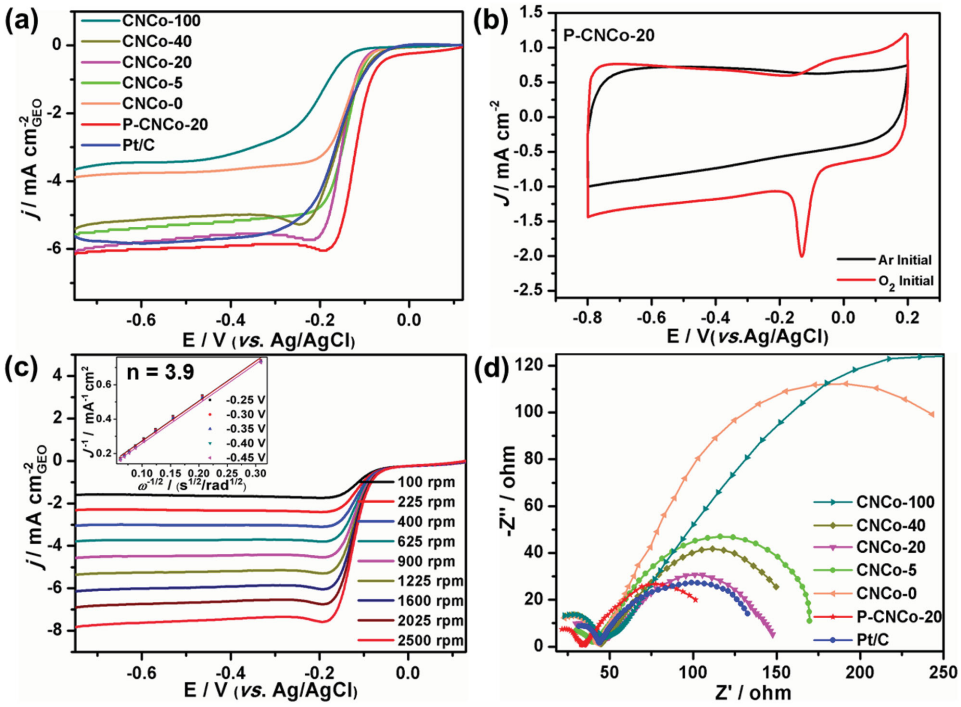

Figure 2. a) LSV curves for different samples in O_2-saturated 0.1 M KOH at a rotation rate of 1600 rpm. b) CV curves of P-CNCo-20 in Ar-saturated and O_2-saturated 0.1 M KOH. c) LSV curves of P-CNCo-20 at different rotation speeds (inset: K-L plots and electron transfer numbers of P-CNCo-20 at different potentials). d) Impedance data for different samples.

voltammetry (CV) curves for all samples exhibit a well-defined cathodic peak clearly at –0.12 ≈ –0.2 V, depicting their electrocatalytic activities for ORR (Figure S13, Table S3, Supporting Information). Among the CNCo-*n* samples, CNCo-20 with the highest reduction peak predicts its superior ORR activity. The linear sweep voltammetry (LSV) data collected on the rotating disk electrode (RDE) indicate that ZIF-8- and ZIF-67-derived carbons present very limited activities (onset potentials of ≈–0.12 and –0.07 V, and half-wave potentials of ≈–0.21 and –0.14 V, respectively), both of which have low diffusion-limited currents (**Figure 2**a, Figure S14a, Table S3, Supporting Information). In sharp contrast, the BMZIF-derived carbon materials, possessing suitable surface area, Co–N_x species and well-dispersed N/Co dopants, exhibit significantly higher ORR activity, among which CNCo-20 with optimized structural attributes is the best (≈–0.08 V for onset potential and ≈–0.15 V for half-wave potential) and even comparable to that of Pt/C (20 wt% Pt, E-TEK).

As expected, the electrocatalytic performance of CNCo-20 can be further boosted upon P doping. The CV curve for P-CNCo-20 displays a nearly rectangular shape, indicating the excellent conductivity with high capacitive current.[7] A pronounced reduction peak is located at ≈–0.12 V in O_2-saturated solution (Figure 2b), superior to those of CNCo-*n* samples. Remarkably, the P-CNCo-20 presents dramatically more positive onset potential (–0.04 V) and half-wave potential (–0.12 V) as well as higher diffusion-limited current density of 6.0 mA cm^{-2} (Figure 2a) against its counterparts and Pt/C (onset potential of ≈–0.04 V, half-wave potential of ≈–0.16 V, and diffusion-limited current density of 5.8 mA cm^{-2}) with the same loading (≈0.1 mg cm^{-2}). To the best of our knowledge, this record of onset/half-wave potential and diffusion-limited current achieved for P-CNCo-20 is among the best in all MOF-derived ORR catalysts as well as other noble-metal free materials reported to date in an alkaline medium (Tables S4 and S5, Supporting Information).[2c–f,6,8] The superb catalytic activity of P-CNCo-20 is assumed to arise from the synergistic effect of high surface area, Co–N_x species, uniform dispersion of N, Co, and P dopants, as well as hierarchical pores in its structure.

To assess the ORR electron-transfer mechanism, RDE measurements have been conducted at various rotation rates, which give the increasing current densities with increasing rotation rates (Figure 2c, Figure S15, Supporting Information). The electron-transfer numbers (*n*) are calculated based on the Koutecky–Levich (K-L) equation, revealing that the different electron-transfer numbers vary from ≈2.3 to 3.9 at –0.25 to –0.4 V for all samples (Figure 2c inset, S16, Supporting Information). The P-CNCo-20 catalyst gives an electron-transfer number of 3.9, which appears similar to that of Pt/C (3.9) and much higher than other reference catalysts. The smaller Tafel slope for P-CNCo-20 than those of other catalysts further demonstrates its superb ORR activity (Figure S17, Supporting Information). Moreover, the electrochemical impedance spectroscopy (EIS) measurements in the ORR region at –0.12 V for various catalysts were conducted. The Nyquist plots indicate that P-CNCo-20 possesses the smallest charge transfer resistance in comparison with Pt/C and other samples (Figure 2d, Figure S18, Supporting Information), which reflects the contribution from its high graphitization degree. All these results

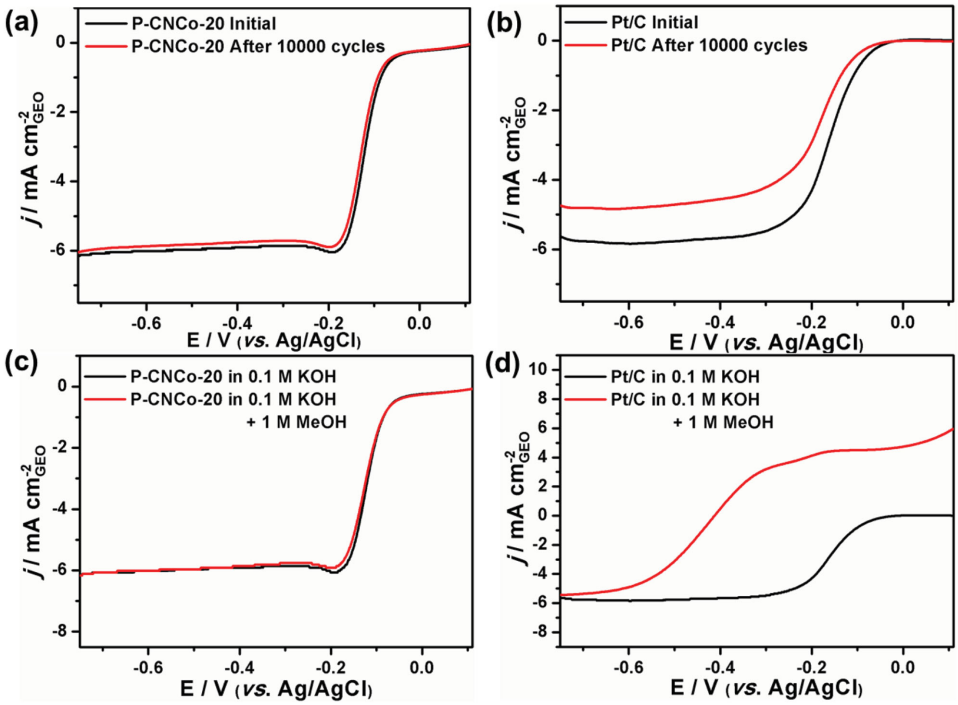

Figure 3. LSV curves of a) P-CNCo-20 and b) commercial Pt/C before and after 10 000 potential cycles in O_2-saturated 0.1 M KOH solution. The LSV curves of c) P-CNCo-20 and d) commercial Pt/C in O_2-saturated 0.1 M KOH without (black curve) and with (red curve) 1 M MeOH (catalyst loading: 0.1 mg cm^{-2}).

highlight the significantly better ORR activity of P-CNCo-20 than that of commercial Pt/C.

In addition to the excellent ORR activity, P-CNCo-20 also exhibits excellent stability and methanol tolerance. The sample was cycled from –0.4 to 0 V at 50 mV s^{-1} in O_2-saturated 0.1 M KOH solution (**Figure 3**a,b, S19, Supporting Information). After continuous 10 000 cycles, the half-wave potential of P-CNCo-20 catalyst is almost maintained with only a negative shift of 5 mV. In contrast, a ≈30 mV negative shift has been observed for Pt/C catalyst, exemplifying the superb stability of P-CNCo-20. Moreover, almost no variation in the LSV curve of P-CNCo-20 can be observed upon the addition of methanol (Figure 3c), totally different from the sharp activity decrease for Pt/C catalyst (Figure 3d). The results here demonstrate that P-CNCo-20 has strong tolerance against crossover effect, making it a promising catalyst for direct methanol fuel cells (Figure S20, Supporting Information).

In summary, bimetallic MOFs have been designed and successfully synthesized as templates/precursors to afford porous carbon with high surface area, high graphitization degree, CoN_x moiety and uniform N dopant by pyrolysis. The resultant CNCo-20 with hierarchical pores and regular shape in nanoscale was exploited as an electrocatalyst that exhibits excellent ORR activity approaching the value of Pt/C. Upon additional P doping, the ORR activity of P-CNCo-20 can be further boosted and surpasses those of Pt/C catalyst and most of non-precious metal materials. It is worth noting that the P-CNCo-20 possesses extraordinary long-term stability and tolerance to methanol in comparison to Pt/C catalyst. The excellent catalytic performance of P-CNCo-20 is believed attributable to the synergistic effect of hierarchical porous structure, high surface area, high graphitization degree, CoN_x active species, as well as uniform dispersion of N, Co, and P dopants. It is expected that this novel and low-cost catalysts templated with MOFs might be extended to other similar systems and hold great promise for advanced electrodes substituting Pt/C in energy storage and conversion.

Experimental Section

Preparation of ZIF-8 Nanocrystals: The synthesis of ZIF-8 nanocrystals was based on a previous procedure with some modifications.[9c] Typically, $Zn(NO_3)_2{\cdot}6H_2O$ (1.68 g) was dissolved in 80 mL of methanol. A mixture of 2-methylimidazole (3.70 g) with 80 mL methanol was added to the above solution with vigorous stirring for 24 h. The product was separated by centrifugation and washed thoroughly with methanol for twice, and finally dried overnight at 50 °C. The ZIF-8 powder was further activated at 200 °C under vacuum for 24 h prior to use.

Preparation of ZIF-67 Nanocrystals: The synthesis of ZIF-67 was based on a previous procedure with modifications.[10b] Typically, $Co(NO_3)_2{\cdot}6H_2O$ (0.45 g) was dissolved in 3 mL of deionized (DI) water; then 2-methylimidazole (5.5 g) in 20 mL of water was added into above solution under vigorously stirred for 6 h at room temperature. The resulting purple precipitates were collected by centrifuging, washed with water and methanol in sequence for at least three times, and finally dried in vacuum at 50 °C overnight. The ZIF-67 powder was further activated at 200 °C under vacuum for 24 h prior to use.

Preparation of BMZIF Nanocrystals: Similar to the synthetic procedure of ZIF-8, typically, the mixture $Zn(NO_3)_2{\cdot}6H_2O$ and $Co(NO_3)_2{\cdot}6H_2O$ with desired molar ratio of Zn^{2+}/Co^{2+} was dissolved in 80 mL of methanol. A mixture of 2-methylimidazole (3.70 g) with 80 mL methanol was added to the above solution with vigorous stirring for 24 h at room temperature

(Scheme S1, Supporting Information). The total molar amount of (Zn + Co) was fixed to be 5.65 mmol. The product was separated by centrifugation and washed thoroughly with methanol for twice, and finally dried overnight at 50 °C. The BMZIF powder was further activated at 200 °C under vacuum for 24 h prior to use.

Preparation of Porous Carbon Materials from BMZIFs: The 500 mg of activated BMZIF powder was heated to 900 °C at a heating rate of 5 °C min^{-1} and carbonized at 900 °C for 2 h under flowing N_2 (80 mL min^{-1}) atmosphere, and cooled to room temperature naturally to obtain porous carbon materials. Then the inactive and unstable Co nanoparticles in product were etched as far as possible with 0.5 M H_2SO_4 aqueous solution at 80 °C for 12 h for twice, and washed thoroughly with lots of water to yield CNCo-*n* catalysts. Finally, the products were dried in vacuum at 120 °C overnight prior to use.

Preparation of P-doped Carbon Material: The 50 mg of porous CNCo-20 or CNCo-100 material obtained above was added into 5 mL of triphenylphosphine (2 mg mL^{-1}) methanol solution. Then the mixture was vigorously stirred under vacuum at room temperature for 24 h. The obtained powder was annealed under nitrogen gas flow at 800 °C in a tubular furnace for 2 h to afford P-CNCo-20 or P-CNCo-100. The product was washed thoroughly with plenty of water and ethanol, and then dried under vacuum for 24 h.

Evaluation of the Catalytic Performance for ORR: All electrochemical measurements were performed in a three-electrode system on an CHI 760E electrochemical workstation (Shanghai Chenhua, China) in 0.1 M KOH electrolyte. A glassy carbon (GC) rotating disk electrode (RDE, PINE, PA, USA) of 5.0 mm in diameter served as the substrate for the working electrode, with the rotating rate varying from 100 to 2500 rpm. A platinum foil and Ag/AgCl (3.5 M KCl) were used as the counter and reference electrodes, respectively. To prepare the working electrode, 2 mg of the catalyst was dispersed in 1 mL of ethanol, and then sonicated for 12 h to form a well dispersed black ink. A certain volume of catalyst ink and 0.02 mL of 5 wt% Nafion solution was then drop-casted onto the glassy carbon surface with a 0.1 mg cm^{-2} loading for all samples, and dried at room temperature. Prior to measurement, an Ar/O_2 flow was used through the electrolyte in the cell for 30 min to saturate it with Ar/O_2. The CV experiments were cycled in Ar- and O_2-saturated 0.1 M aqueous KOH electrolyte solutions with a scan rate of 20 mV s^{-1}. RDE tests were measured in O_2-saturated 0.1 M KOH at room temperature with a sweep rate of 20 mV s^{-1} and different speed rates (100–2500 rpm). For comparison, Pt/C (20 wt% platinum, E-TEK) was conducted on the same electrochemical tests.

For the ORR at a RDE, the electron transfer numbers can be calculated with Koutecky–Levich equations

$$\frac{1}{j} = \frac{1}{j_L} + \frac{1}{j_K} = \frac{1}{B\omega^{1/2}} + \frac{1}{j_K} \quad (1)$$

$$B = 0.62nFC_0(D_0)^{2/3}\nu^{-1/6} \quad (2)$$

$$j_K = nFkC_0 \quad (3)$$

where j is the measured current density; j_K and j_L are the kinetic and diffusion-limiting current densities, respectively; ω is the angular velocity of the disk (= 2πN, N is the linear rotation speed); n represents the overall number of electrons transferred in oxygen reduction; F is the Faraday constant (F = 96485 C mol^{-1}); C_0 is the bulk concentration of O_2 (1.2×10^{-6} mol cm^{-3}); D_0 is the diffusion coefficient of O_2 in 0.1 M KOH electrolyte (1.9×10^{-5} cm^2 s^{-1}); ν is the kinematics viscosity for electrolyte, and k is the electron-transferred rate constant.

Supporting Information

Supporting Information is available from the Wiley Online Library or from the author.

Acknowledgements

Y.-Z.C. and C.W contributed equally to this work. This work was supported by the NSFC (21371162, 51301159, 21473166), the 973 program (2014CB931803), NSF of Anhui Province (1408085MB23, 1508085MB24), the Recruitment Program of Global Youth Experts, and the Fundamental Research Funds for the Central Universities (WK2060190026, WK2060190025).

Received: May 14, 2015
Revised: June 3, 2015
Published online: July 20, 2015

[1] a) S. H. Joo, S. J. Choi, I. Oh, J. Kwak, Z. Liu, O. Terasaki, R. Ryoo, *Nature* **2001**, *412*, 169; b) Z. Ma, T. Kyotani, Z. Liu, O. Terasaki, A. Tomita, *Chem. Mater.* **2001**, *13*, 4413; c) J. Lee, Kim, T. Hyeon, *Adv. Mater.* **2006**, *18*, 2073; d) K. M. Thomas, *Catal. Today* **2007**, *120*, 389; e) Z. Yang, Y. Xia, R. Mokaya, *J. Am. Chem. Soc.* **2007**, *129*, 1673; f) C. D. Liang, Z. J. Li, S. Dai, *Angew. Chem. Int. Ed.* **2008**, *47*, 3696; g) J. Tang, J. Liu, N. L. Torad, T. Kimura, Y. Yamauchi, *Nano Today* **2014**, *9*, 305; h) Y. Jiao, Y. Zheng, M. Jaroniec, S. Z. Qiao, *J. Am. Chem. Soc.* **2014**, *136*, 4394.

[2] a) C. O. Ania, V. Khomenko, E. Raymundo-Pinero, J. B. Parra, F. Beguin, *Adv. Funct. Mater.* **2007**, *17*, 1828; b) D. Hulicova-Jurcakova, A. M. Puziy, O. I. Poddubnaya, F. Suarez-Garcia, J. M. D. Tascon, G. Q. Lu, *J. Am. Chem. Soc.* **2009**, *131*, 5026; c) K. P. Gong, F. Du, Z. H. Xia, M. Durstock, L. M. Dai, *Science* **2009**, *323*, 760; d) D.-S. Yang, D. Bhattacharjya, S. Inamdar, J. Park, J.-S. Yu, *J. Am. Chem. Soc.* **2012**, *134*, 16127; e) Y. Zheng, Y. Jiao, M. Jaroniec, Y. Jin, S. Z. Qiao, *Small* **2012**, *8*, 3550; f) W. Wei, H. Liang, K. Parvez, X. Zhuang, X. Feng, K. Müllen, *Angew. Chem. Int. Ed.* **2014**, *53*, 1570.

[3] a) L. Yang, S. Jiang, Y. Zhao, L. Zhu, S. Chen, X. Wang, W. Qiang, J. Ma, Y. Ma, Z. Hu, *Angew. Chem. Int. Ed.* **2011**, *50*, 7132; b) H. Tang, H. Yin, J. Wang, N. Yang, D. Wang, Z. Tang, *Angew. Chem. Int. Ed.* **2013**, *52*, 5585.

[4] a) J. R. Long, O. M. Yaghi, *Chem. Soc. Rev.* **2009**, *38*, 1213; b) H.-C. Zhou, J. R. Long, O. M. Yaghi, *Chem. Rev.* **2012**, *112*, 673; c) H.-C. Zhou, S. Kitagawa, *Chem. Soc. Rev.* **2014**, *43*, 5415.

[5] a) B. Liu, H. Shioyama, T. Akita, Q. Xu, *J. Am. Chem. Soc.* **2008**, *130*, 5390; b) H.-L. Jiang, B. Liu, Y.-Q. Lan, K. Kuratani, T. Akita, H. Shioyama, F. Zong, Q. Xu, *J. Am. Chem. Soc.* **2011**, *133*, 11854; c) A. Almasoudi, R. Mokaya, *J. Mater. Chem.* **2012**, *22*, 146; d) M. Hu, J. Reboul, S. Furukawa, N. L. Torad, Q. M. Ji, P. Srinivasu, K. Ariga, S. Kitagawa, Y. Yamauchi, *J. Am. Chem. Soc.* **2012**, *134*, 2864; e) K. Jayaramulu, N. Kumar, A. Hazra, T. K. Maji, C. N. R. Rao, *Chem.-Eur. J.* **2013**, *19*, 6966; f) G. Srinivas, V. Krungleviciute, Z.-X. Guo, T. Yildirim, *Energy Environ. Sci.* **2014**, *7*, 335; g) F. Zheng, Y. Yang, Q. Chen, *Nat. Commun.* **2014**, *6*, 5261; h) J. Tang, R. R. Salunkhe, J. Liu, N. L. Torad, M. Imura, S. Furukawa, Y. Yamauchi, *J. Am. Chem. Soc.* **2015**, *137*, 1572.

[6] a) S. Ma, G. A. Goenaga, A. V. Call, D.-J. Liu, *Chem.-Eur. J.* **2011**, *17*, 2063; b) P. Su, H. Xiao, J. Zhao, Y. Yao, Z. Shao, C. Li, Q. Yang, *Chem. Sci.* **2013**, *4*, 2941; c) P. Zhang, F. Sun, Z. Xiang, Z. Shen, J. Yun, D. Cao, *Energy Environ. Sci.* **2014**, *7*, 442; d) W. Zhang, Z.-Y. Wu, H.-L. Jiang, S.-H. Yu, *J. Am. Chem. Soc.* **2014**, *136*, 14385; e) A. Aijaz, N. Fujiwara, Q. Xu, *J. Am. Chem. Soc.* **2014**, *136*, 6790; f) D. Zhao, J.-L. Shui, L. R. Grabstanowicz, C. Chen, S. M. Commet, T. Xu, J. Lu, D.-J. Liu, *Adv. Mater.* **2014**, *26*, 1093; g) S. Zhao, H. Yin, L. He, L. Du, K. Zhao, L. Chang, G. Yin, H. Zhao, S. Liu, Z. Tang, *ACS Nano* **2014**, *8*, 12660; h) X. Wang, J. Zhou, H. Fu, W. Li, X. Fan, G. Xin, J. Zheng, X. Li, *J. Mater. Chem. A.* **2014**, *2*, 14064; i) X. Wang, J. Zhou, H. Fu, W. Li, X. Fan, G. Xin, J. Zheng, X. Li, *J. Mater. Chem.*

A **2014**, *2*, 14064; j) Q. Lin, X. Bu, A. Kong, C. Mao, X. Zhao, F. Bu, P. Feng, *J. Am. Chem. Soc.* **2015**, *137*, 2235; k) H. Zhong, J. Wang, Y. Zhang, W. Xu, W. Xing, D. Xu, Y. Zhang, X. Zhang, *Angew. Chem. Int. Ed.* **2014**, *53*, 14235; l) W. Xia, R. Zou, L. An, D. Xia, S. Guo, *Energy Environ. Sci.* **2015**, *8*, 568; m) W. Xia, A. Mahmood, R. Zou, Q. Xu, Energy Environ. Sci., *2015*, DOI: 10.1039/C5EE00762C.

[7] a) B. C. H. Steele, A. Heinzel, *Nature* **2001**, *414*, 345; b) B. Lim, M. J. Jiang, P. H. C. Camargo, E. C. Cho, J. Tao, X. M. Lu, Y. M. Zhu, Y. N. Xia, *Science* **2009**, *324*, 1302; c) V. Mazumder, M. Chi, K. L. More, S. Sun, *J. Am. Chem. Soc.* **2010**, *132*, 7848; d) Y. Liang, Y. Li, H. Wang, J. Zhou, J. Wang, T. Regier, H. Dai, *Nat. Mater.* **2011**, *10*, 780; e) D. F. van der Vliet, C. Wang, D. Tripkovic, D. Strmcnik, X. F. Zhang, M. K. Debe, R. T. Atanasoski, N. M. Markovic, V. R. Stamenkovic, *Nat. Mater.* **2012**, *11*, 1051; f) A. Holewinski, J.-C. Idrobo, S. Linic, *Nat. Chem.* **2014**, *6*, 828.

[8] a) M. Lefvre, E. Proietti, F. Jaouen, J.-P. Dodelet, *Science* **2009**, *324*, 71; b) G. Wu, K. L. More, C. M. Johnston, P. Zelenay, *Science* **2011**, *332*, 443; c) E. Proietti, F. Jaouen, M. Lefèvre, N. Larouche, J. Tian, J. Herranz, J.-P. Dodelet, *Nat. Commun.* **2011**, *2*, 416; d) A. L. Bouwkamp-Wijnoltza, W. Visschera, J. A. R. van Veena, S. C. Tang, *Electrochim. Acta* **1999**, *45*, 379; e) H.-J. Zhang, X. Yuan, W. Wen, D.-Y. Zhang, L. Sun, Q.-Z. Jiang, Z.-F. Ma, *Electrochem. Commun.* **2009**, *11*, 206; f) R. Liu, C. von Malotki, L. Arnold, N. Koshino, H. Higashimura, M. Baumgarten, K. Müllen, *J. Am. Chem. Soc.* **2011**, *133*, 10372; g) Z. Chen, D. Higgins, A. Yu, L. Zhang, J. Zhang, *Energy Environ. Sci.* **2011**, *4*, 3167; h) Y. Hou, Z. Wen, S. Cui, S. Ci, S. Mao, J. Chen, *Adv. Funct. Mater.* **2015**, *25*, 872.

[9] a) K. S. Park, Z. Ni, A. P. Côté, J. Y. Choi, R. Huang, F. J. Uribe-Romo, H. K. Chae, M. O'Keeffe, O. M. Yaghi, *Proc. Natl. Acad. Sci. USA* **2006**, *103*, 10186; b) X.-C. Huang, Y.-Y. Lin, J.-P. Zhang, X.-M. Chen, *Angew. Chem. Int. Ed.* **2006**, *45*, 1557; c) S. R. Venna, J. B. Jasinski, M. A. Carreon, *J. Am. Chem. Soc.* **2010**, *132*, 18030.

[10] a) R. Banerjee, A. Phan, B. Wang, C. Knobler, H. Furukawa, M. O'Keeffe, O. M. Yaghi, *Science* **2008**, *319*, 939; b) J. Qian, F. Sun, L. Qin, *Mater. Lett.* **2012**, *82*, 220.

[11] a) Z. Yan, M. Cai, P. K. Shen, *J. Mater. Chem.* **2012**, *22*, 2133; b) J. Tang, T. Wang, X. Pan, X. Sun, X. Fan, Y. Guo, H. Xue, J. He, *J. Phys. Chem. C* **2013**, *117*, 16896.

[12] a) T. S. Olson, P. Svitlana, A. Plamen, *J. Phys. Chem. C.* **2010**, *114*, 5049; b) A. Morozan, P. Jégou, B. Jousselme, S. Palacin, *Phys. Chem. Chem. Phys.* **2011**, *13*, 21600.